Vehicle Impact on the Deck Slab of Concrete Box-Girder Bridges due to Damaged Expansion Joints

Lu Deng, Ph.D., M. ASCE[1]; Wangchen Yan[2]; and Quanjun Zhu[3]

Abstract: Expansion joints will experience increasing deterioration and damage under repeating vehicle loading. A severely damaged expansion joint will induce significant dynamic vehicle load effects on the bridge deck near the expansion joint, whereas it may not cause such a large effect on the global bridge responses, e.g., deflection and bending moment at the bridge midspan. The impact factors (IMs) in bridge design codes are usually determined from global bridge responses. Therefore, it may be inappropriate to use the IMs in bridge design codes for the design of deck slabs for which the transverse bending moment is usually the controlling internal force. In this study, a three-dimensional vehicle-bridge model is used to study vehicle impact on the deck slab of prestressed concrete box-girder bridges caused by damaged expansion joints. Results show that the damage condition of expansion joints has a significant effect on the vehicle impact on the bridge deck slab, whereas it has a limited effect on the global bridge responses, especially for long bridges. The relationships between the vehicle impact on the deck slab and a few important parameters are also investigated, and some useful conclusions are obtained. **DOI: 10.1061/(ASCE)BE.1943-5592.0000796.**

Author keywords: Local impact factor; Damaged expansion joint; Concrete box-girder bridge; Vehicle–bridge coupled model.

Introduction

Expansion joints have been widely used on bridges to allow for the longitudinal movement of bridge girders. Under repeating vehicle loading, expansion joints will experience increasing deterioration and damage. The life span of most expansion joints is shorter than 10 years, which is usually below their design life (Lima and de Brito 2009). Damaged expansion joints can induce significant vehicle vibration and therefore increase the impact of vehicles on the bridge deck (Kim et al. 2004; González et al., 2011; Kim et al. 2007).

The term *impact factor* (also referred to as *dynamic load allowance*), usually denoted by IM, has been used in bridge design codes to represent the increment of bridge static response due to dynamic vehicle loading. The IMs in many bridge design codes were traditionally determined from global bridge responses. For example, the IM adopted in the AASHTO (1994) LRFD code was based on the work by Hwang and Nowak (1991) in which the bridge midspan deflection was used to calculate the dynamic load factor. However, the controlling internal force of the bridge deck is usually the transverse bending moment, of which the dynamic increment may not be accurately represented by the IMs in the bridge codes, which are determined from global bridge responses. Furthermore, damaged expansion joints could significantly increase the vehicle impact on the deck slab near the expansion joints (Kim and Kawatani 2005; Kim et al. 2007). Kim and Kawatani (2005) further suggested that the IM used for the design of deck slabs should be based on the responses at the cross section close to the expansion joint. As a result, it may be inappropriate to apply the IMs in the bridge design codes to the design or evaluation of deck slabs (Huang 2013), especially near the expansion joints.

This study first adopted a model of expansion joints from the literature. A three-dimensional (3D) vehicle–bridge coupled model was then developed to study the impact of vehicles on the deck slabs of prestressed concrete box-girder bridges due to damaged expansion joints. The IMs of the deck slab based on the transverse bending moment and the global IMs based on the deflection and longitudinal bending moment at the bridge midspan were both calculated and compared. A parametric study was also conducted to investigate the relationship between the IMs of the deck slab and a few important parameters including the damage condition of the expansion joint, bridge span length, road-surface condition and vehicle speed.

Numerical Models

Bridge Models

In the present study, five prestressed concrete box-girder bridges were selected according to the Segmental Box Girder Standards by the AASHTO-PCI-ASBI (1997). These bridges have span lengths ranging from 24 m to 56 m and are good representatives of the simply supported prestressed concrete box-girder bridges in the United States. All five bridges have the same cross sections and two 0.40-m-thick end diaphragms. The bridge deck width and girder depth are 11.1 m and 2.4 m, respectively. Fig. 1 shows the cross section of the five bridges. In this study, the bridges were modeled using solid elements with the *ANSYS* program. Modal analysis was performed on these bridge models, and the natural frequencies and mode shapes were obtained. Table 1 summarizes the primary parameters of the five bridges and the natural frequencies obtained from the modal analysis.

[1]Professor, College of Civil Engineering, Hunan Univ., Changsha, Hunan 410082, China (corresponding author). E-mail: denglu@hnu.edu.cn

[2]Research Assistant, College of Civil Engineering, Hunan Univ., Changsha, Hunan 410082, China. E-mail: ywchen92@163.com

[3]Senior Engineer, Hunan Communications Research Institute, Changsha, Hunan 410015, China. E-mail: jtjr@foxmail.com

Note. This manuscript was submitted on November 6, 2014; approved on March 20, 2015; published online on June 18, 2015. Discussion period open until November 18, 2015; separate discussions must be submitted for individual papers. This technical note is part of the ***Journal of Bridge Engineering***, © ASCE, ISSN 1084-0702/06015006(9)/$25.00.

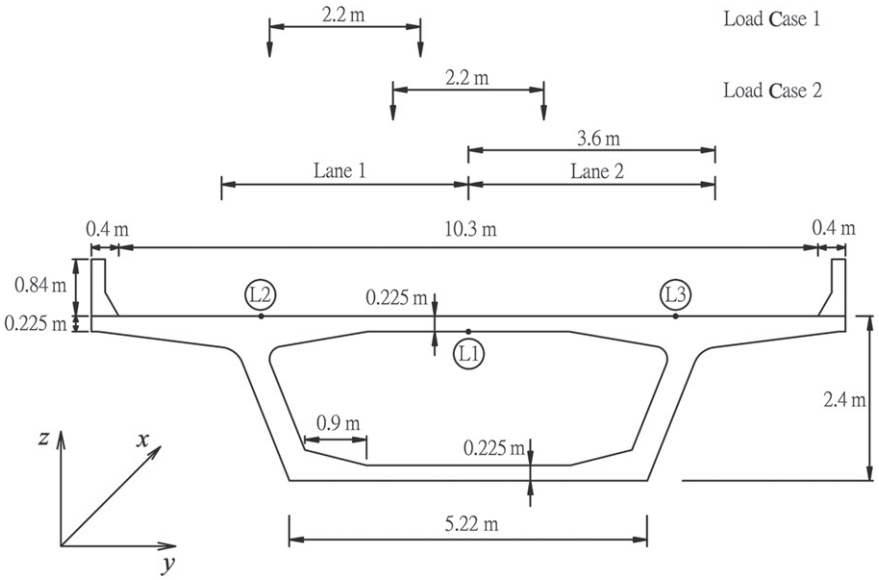

Fig. 1. Cross section of bridges and load cases

Table 1. Detailed Properties of the Five Bridges

Bridge number	Span length (m)	Natural frequency (Hz)	Cross section	
			Area (m^2)	Moment of inertia (m^4)
1	24	7.92	6.395	5.085
2	32	4.70	6.395	5.085
3	40	3.09	6.395	5.085
4	48	2.18	6.395	5.085
5	56	1.61	6.395	5.085

Vehicle Model

For vehicle loading, the HS20-44 truck, which is a major design vehicle in the AASHTO bridge-design specifications (AASHTO 2012), was adopted in the present study. Fig. 2 shows the analytical model of this truck, which consists of a series of masses, springs, and dampers (Shi et al. 2008). Table 2 provides the major parameters of the truck model.

Single-point tire models have been widely adopted for vehicle tire models in simulating bridge–vehicle interactions because of their simplicity (Wang and Huang 1992; Shi et al. 2008; Deng and Cai 2010a). However, because a tire makes contact with the road surface over a footprint area instead of a single point, the use of a single-point tire model may lead to amplified vibrations, especially under distressed road-surface condition (Yin et al. 2010). Thus, the tire model adopted in this study consists of a number of uniformly distributed points, each of which is represented by a spring and a damper that are in contact with the road surface. The stiffness and damping coefficient values of each contact point in this new tire model are therefore the values of the single-point tire model, summarized in Table 2, divided by the total number of contact points (six, based on a convergence test in this study) adopted for each tire. These points span a length of 25.4 cm as per the suggestion of the AASHTO (2012) LRFD code.

Road-Surface Profile

The road-surface profile, usually treated as a random process, can be described by a power spectral density (PSD) function. A modified PSD function (Wang and Huang 1992) was adopted in this study

$$\varphi(n) = \varphi(n_0)\left(\frac{n}{n_o}\right)^{-2} (n_1 < n < n_2) \tag{1}$$

where n = spatial frequency (cycle/m); n_0 = discontinuity frequency of 0.5π (cycle/m); $\varphi(n_0)$ = roughness coefficient (m^3/cycle) depending on the road-surface conditions; and n_1 and n_2 = lower and upper cut-off frequencies, respectively. ISO (1995) classified road-surface conditions using different roughness coefficients. In the present study, roughness coefficients of 5×10^{-6}, 20×10^{-6}, 80×10^{-6}, and 256×10^{-6} according to the ISO (1995) were used for very good, good, average, and poor road-surface conditions, respectively.

A road-surface profile can then be generated by an inverse Fourier transformation with the PSD function and can be expressed as follows:

$$r(X) = \sum_{k=1}^{N} \sqrt{2\varphi(n_k)\Delta n}\, \cos(2\pi n_k X + \theta_k) \tag{2}$$

where X = position of the point of interest on the road in the longitudinal direction; θ_k = random phase angle that has a uniform distribution from 0 to 2π; and n_k = wave number (cycle/m).

Expansion Joint

On the basis of a review of expansion joints, González et al. (2011) proposed an expansion joint model. This model was adopted in the present study, as shown in Fig. 3. The expansion joint in Fig. 3 has a trapezoidal shape and a width of 20 cm at the road-surface level. On the basis of the survey results of expansion joints on the national roadway bridges in Japan (Kim and Kawatani 2005; Kim et al. 2007) and Portugal (Lima and de Brito 2009), three different values for the height h, namely, 0, 2, and 4 cm, were adopted in this study to represent three damage conditions of the expansion joint: no damage, moderate damage, and severe damage, respectively. Fig. 4 shows a good road-surface profile with an expansion joint that has moderate damage. It can be

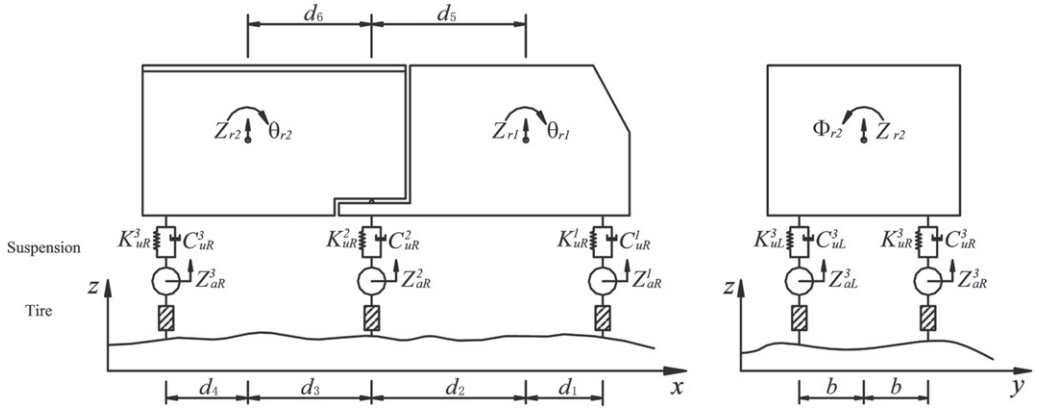

Fig. 2. Analytical model of the HS20-44 truck

Table 2. Major Parameters of the Truck Model Under Study (HS20)

Parameter	Value
Mass of Truck Body 1	2,612 (kg)
Pitching moment of inertia of Truck Body 1	2,022 (kg · m^2)
Rolling moment of inertia of Truck Body 1	8,544 (kg · m^2)
Mass of Truck Body 2	26,113 (kg)
Pitching moment of inertia of Truck Body 2	33,153 (kg · m^2)
Rolling moment of inertia of Truck Body 2	181,216 (kg · m^2)
Mass of first axle suspension	490 (kg)
Upper spring stiffness of first axle	242,604 (N/m)
Upper damper coefficient of first axle	2,190 (N · s/m)
Lower spring stiffness of first axle	875,082 (N/m)
Lower damper coefficient of first axle	2,000 (N · s/m)
Mass of second axle suspension	808 (kg)
Upper spring stiffness of second axle	1,903,172 (N/m)
Upper damper coefficient of second axle	7,882 (N · s/m)
Lower spring stiffness of second axle	3,503,307 (N/m)
Lower damper coefficient of second axle	2,000 (N · s/m)
Mass of third axle suspension	653 (kg)
Upper spring stiffness of third axle	1,969,034 (N/m)
Upper damper coefficient of third axle	7,182 (N · s/m)
Lower spring stiffness of the third axle	3,507,429 (N/m)
Lower damper coefficient of third axle	2,000 (N · s/m)
d_1	1.698 (m)
d_2	2.569 (m)
d_3	1.984 (m)
d_4	2.283 (m)
d_5	2.215 (m)
d_6	2.338 (m)
b	1.1 (m)

clearly seen that the expansion joint is located at the entrance of the bridge.

Vehicle–Bridge Coupled Model

The equations of motion for a bridge and vehicle can be written as follows:

$$[M_b]\{\ddot{d}_b\} + [C_b]\{\dot{d}_b\} + [K_b]\{d_b\} = \{F_b\} \tag{3}$$

$$[M_v]\{\ddot{d}_v\} + [C_v]\{\dot{d}_v\} + [K_v]\{d_v\} = \{F_G\} + \{F_v\} \tag{4}$$

where $[M_b]$, $[C_b]$, and $[K_b]$ = mass, damping, and stiffness matrices of the bridge, respectively; $[M_v]$, $[C_v]$, and $[K_v]$ = mass, damping, and stiffness matrices of the vehicle, respectively; $\{d_b\}$ and $\{d_v\}$ = displacement vector of the bridge and vehicle, respectively; $\{F_b\}$ and $\{F_v\}$ = wheel–road contact force vectors acting on the bridge and vehicle, respectively; and $\{F_G\}$ = gravity–force vector of the vehicle.

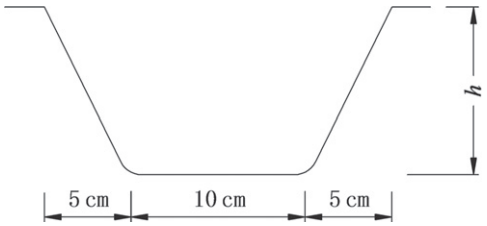

Fig. 3. Model of expansion joint

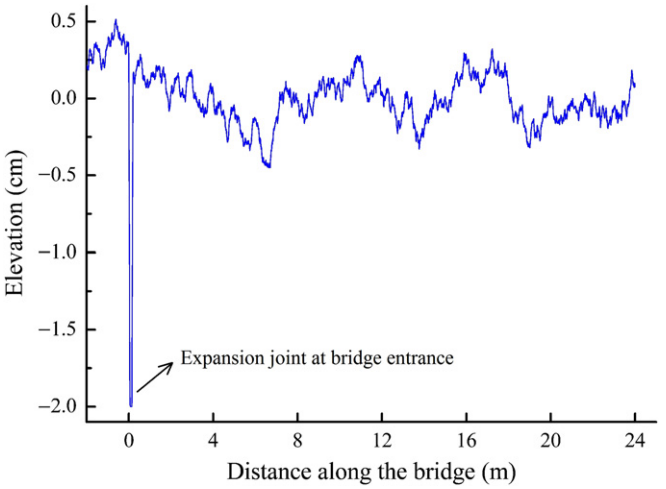

Fig. 4. A good road-surface profile with an expansion joint with moderate damage

On the basis of the displacement relationship and interaction force relationship at the wheel–road contact points, Eqs. (3) and (4) can be combined into one coupled equation as follows:

$$\begin{bmatrix} M_b & \\ & M_v \end{bmatrix} \begin{Bmatrix} \ddot{d}_b \\ \ddot{d}_v \end{Bmatrix} + \begin{bmatrix} C_b + C_{b-b} & C_{b-v} \\ C_{v-b} & C_v \end{bmatrix} \begin{Bmatrix} \dot{d}_b \\ \dot{d}_v \end{Bmatrix} + \begin{bmatrix} K_b + K_{b-b} & K_{b-v} \\ K_{v-b} & K_v \end{bmatrix} \begin{Bmatrix} d_b \\ d_v \end{Bmatrix} = \begin{Bmatrix} F_{b-r} \\ F_{b-r} + F_G \end{Bmatrix} \tag{5}$$

where C_{b-b}, C_{b-v}, C_{v-b}, K_{b-b}, K_{b-v}, K_{v-b}, F_{b-r}, and F_{b-r} = terms caused by the vehicle–bridge interaction. As the vehicle crosses the bridge, the positions of the contact points change as do these interaction terms.

Using the modal superposition technique, Eq. (5) can be simplified as follows:

$$\begin{bmatrix} I & \\ & M_v \end{bmatrix} \begin{Bmatrix} \ddot{\xi}_b \\ \ddot{d}_v \end{Bmatrix} + \begin{bmatrix} 2\omega_i\eta_i I + \Phi_b^T C_{b-b}\Phi_b & \Phi_b^T C_{b-v} \\ C_{v-b}\Phi_b & C_v \end{bmatrix} \begin{Bmatrix} \dot{\xi}_b \\ \dot{d}_v \end{Bmatrix} + \begin{bmatrix} \omega_i^2 I + \Phi_b^T K_{b-b}\Phi_b & \Phi_b^T K_{b-v} \\ K_{v-b}\Phi_b & K_v \end{bmatrix} \begin{Bmatrix} \xi_b \\ d_v \end{Bmatrix} = \begin{Bmatrix} \Phi_b^T F_{b-r} \\ F_{b-r} + F_G \end{Bmatrix} \tag{6}$$

Eq. (6) contains only the modal properties of the bridge and the mechanical parameters of the vehicles. As a result, the complexity of solving the coupled equations is greatly reduced. The fourth-order Runge–Kutta method was adopted to solve Eq. (6) in the time domain. For more details of the bridge–vehicle coupled system, see Deng and Cai (2010a).

Numerical Simulations

Problem Description

The primary purpose of this study is to investigate the vehicle impact on bridge deck slabs due to damaged expansion joints and compare it with the impact on global bridge responses. Vehicle impact is studied in terms of the IM, defined as follows in the present study:

$$IM = \frac{R_{dyn} - R_{sta}}{R_{sta}} \tag{7}$$

where R_{dyn} and R_{sta} = maximum dynamic and static responses of the target point on the bridge, respectively.

For convenience, two terms, namely, the local IM of the deck slab and the global IM, will be used to differentiate the two concepts discussed previously. The local IM of the deck slab is calculated using the local transverse bending moment of the deck slab (about the x-axis indicated in Fig. 1), whereas the global IM for bending moment is calculated using the global bending moment of the main girder (about the y-axis indicated in Fig. 1). Because it is usually the controlling internal force for bridge components (González et al. 2011; Brühwiler and Herwig 2008), the bending moment was selected as the only internal force to calculate the IMs, for both the local IM of the deck slab and the global IM. In addition, the bridge midspan deflection was also selected for calculating the global IM because it has been widely used by bridge engineers and researchers. To summarize, the local IM of deck slab will be calculated from the transverse bending moment of the deck slab, and the global IM will be calculated from the deflection and longitudinal bending moment at the bridge midspan.

Kim and Kawatani (2005) suggested that because of the presence of damaged expansion joints, the IM used for the design of deck slabs should be based on the responses at the cross section close to the expansion joints. It is therefore necessary to first select the cross section to be used for calculating the deck response.

In this study, two load cases were adopted for vehicle loading, in which a single truck was set to travel along the centerline of Lane 1 and the centerline of the deck slab, respectively, as shown in Fig. 1. Fig. 1 also shows the points of interest used for calculating the local IMs of the deck slabs, which were marked as L1, L2, and L3, where the letter L denotes local. Because the transverse bending moment at L2 is certainly no less than the bending moment at L3

Table 3. Longitudinal Positions of Points L1 and L2 on the Five Bridges Under the Two Load Cases

		Load Case 1		Load Case 2	
Point of interest	Bridge span length (m)	Distance to expansion joint (m)	Static transverse strain	Distance to expansion joint (m)	Static transverse strain
L1	24	5.2	1.77×10^{-5}	6	2.04×10^{-5}
	32		1.79×10^{-5}		2.05×10^{-5}
	40		1.79×10^{-5}		2.06×10^{-5}
	48		1.80×10^{-5}		2.06×10^{-5}
	56		1.80×10^{-5}		2.07×10^{-5}
L2	24	4.4	1.03×10^{-5}	4.4	1.36×10^{-5}
	32		1.05×10^{-5}		1.37×10^{-5}
	40		1.05×10^{-5}		1.38×10^{-5}
	48		1.06×10^{-5}		1.38×10^{-5}
	56		1.06×10^{-5}		1.39×10^{-5}

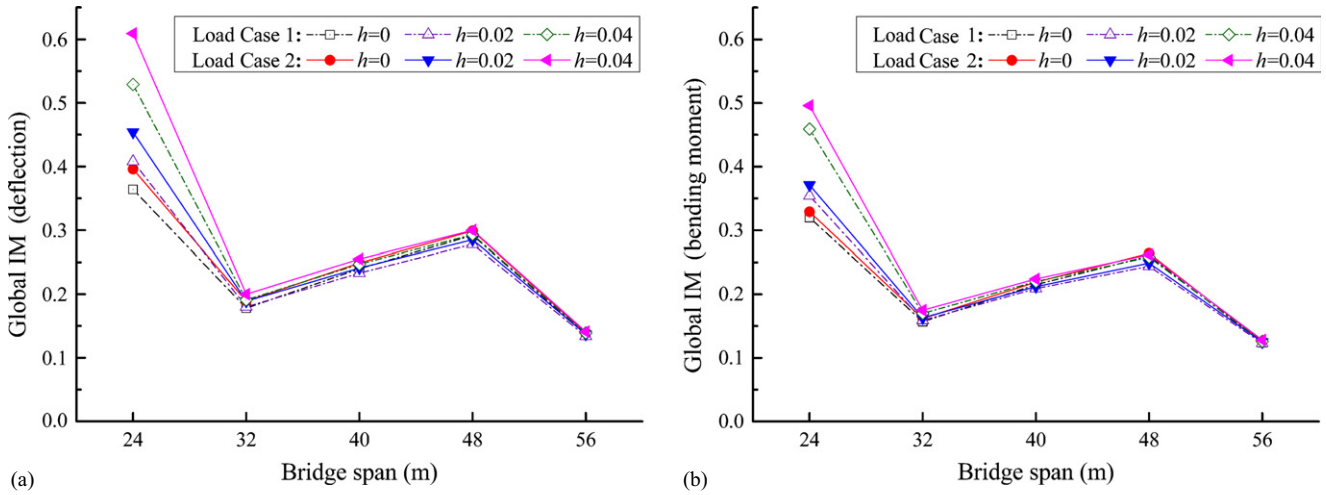

Fig. 5. Global IMs of different bridges under the two load cases: (a) midspan deflection; (b) midspan longitudinal bending moment

under both load cases, only L2 was investigated. As a result, L1 and L2 represent the points of interest for investigating the positive and negative transverse bending moments of the deck slab, respectively.

To determine the longitudinal position of Points L1 and L2 on the bridge for calculating the deck response, static analysis was performed for the two load cases in which the truck moved across the bridge step by step, and the static strains at L1 and L2 at each step were recorded. Then, the longitudinal positions at which the static transverse strains at L1 and L2 reached their maxima were selected as the positions for calculating the local IMs of the deck slab. The reason why the static transverse strains gradually increase as the truck moves across the bridge is due to the influence of the end diaphragm on the transverse bending moments of the deck slab near the end support. However, with a certain distance from the end support, the transverse strains on the deck slab will become stable as the influence of the end diaphragm vanishes. Table 3 shows the maximum static transverse strains and the corresponding positions of the points selected for calculating the local IMs under the two load cases for all five bridges.

In the following sections, the effect of different parameters, including the damage condition of the expansion joint, bridge span length, vehicle speed, and road-surface condition on the IMs will be investigated. Five vehicle speeds (30, 45, 60, 75, and 90 km/h), four road-surface conditions [very good, good, average, and poor according to the ISO (1995)], and three damage conditions [no damage ($h = 0$ cm), moderate damage ($h = 2$ cm), and severe damage ($h = 4$ cm)] were investigated. Under each combination of these parameters, the vehicle–bridge analysis program was set to run 20 times with 20 randomly generated road-surface profiles under the given road-surface conditions. Then, the average value of the 20 IMs obtained was used in the results analysis.

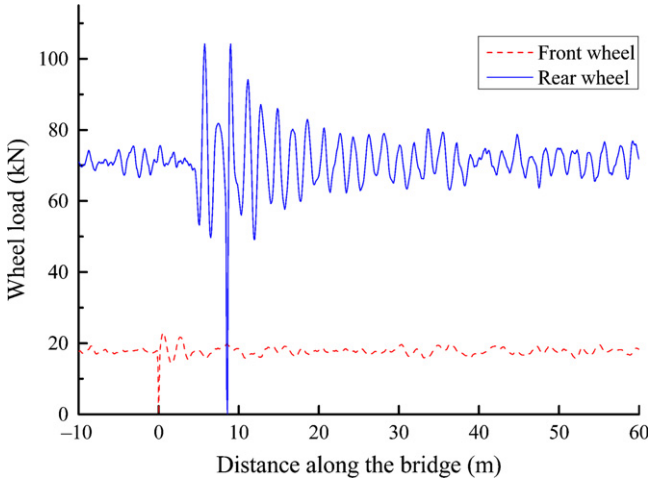

Fig. 6. Wheel-load time history before and after the truck passes a severely damaged expansion joint

Effects of Damage Condition of Expansion Joint and Bridge-Span Length

The global IMs of all five bridges, calculated from the deflection and longitudinal bending moment (about the y-axis indicated in Fig. 1) at the bridge midspan, were obtained and are shown in Fig. 5. As shown in Fig. 5, the global IMs do not necessarily decrease with the increase of the bridge-span length. In fact, the IMs reach two local maxima at the bridge span lengths of 24 and 48 m, respectively. Further investigation revealed that the natural frequencies of these two bridges (7.92 and 2.18 Hz) are close to the sixth and second natural frequencies of the truck (7.82 and 2.14 Hz, respectively), which may have caused the resonance. Similar findings were also observed by other researchers (Green et al. 1995; Schwarz and Laman 2001; Ding et al. 2009). In addition, it can be observed that the effect of the damage condition of expansion joint on the global IMs is notable on the 24-m span bridge, whereas this effect vanishes quickly as the bridge-span length increases. This occurs because the dynamic load effect initially induced by the damaged expansion joint decreases quickly because of vehicle damping as the vehicle moves, as shown in Fig. 6. For relatively long bridges, the dynamic load effect will have been reduced significantly by the time the truck reaches the midspan.

Using an average road-surface condition, the local IMs of the deck slab at the selected points are plotted against the bridge-span length under different damage conditions of the expansion joint, for both load cases, in Fig. 7. From this figure, the following can be observed: (1) the local IMs of the deck slab increase significantly as the damage condition of the expansion joint becomes more severe; the average local IMs may exceed 0.33, the value

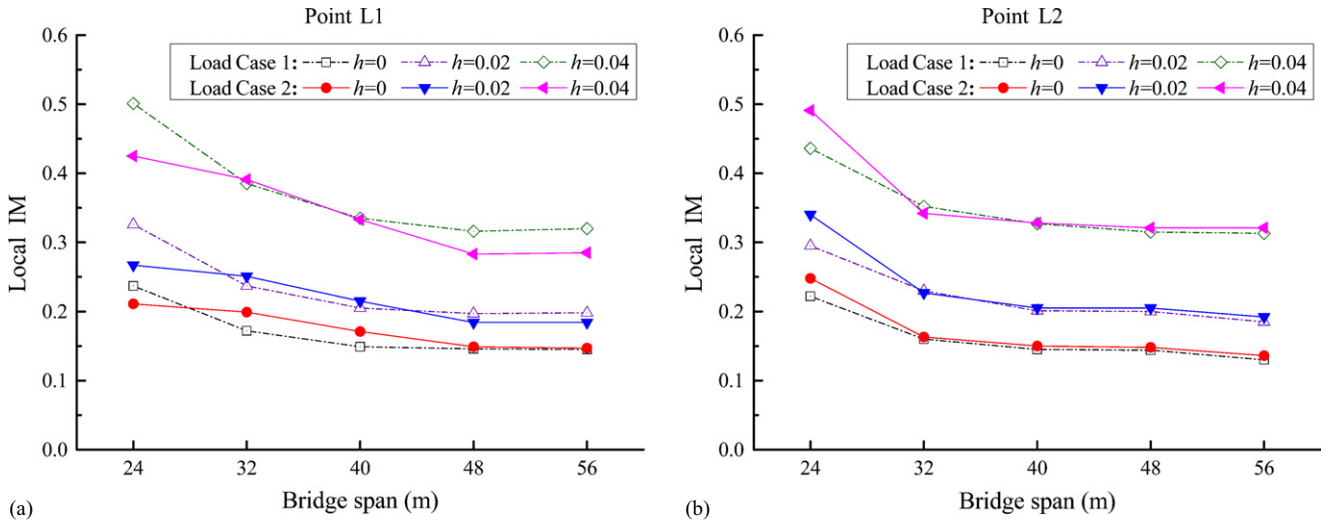

Fig. 7. Local IMs of the deck slab of different bridges under the two load cases: (a) Point L1; (b) Point L2

specified in the AASHTO (2012) LRFD code, under the severely damaged expansion joint, especially for short bridges; and (2) the local IMs decrease significantly from the 24-m span bridge to the 32-m span bridge after which the IMs decrease slowly as the bridge span increases, which is different from the trend with the global IMs observed in Fig. 5.

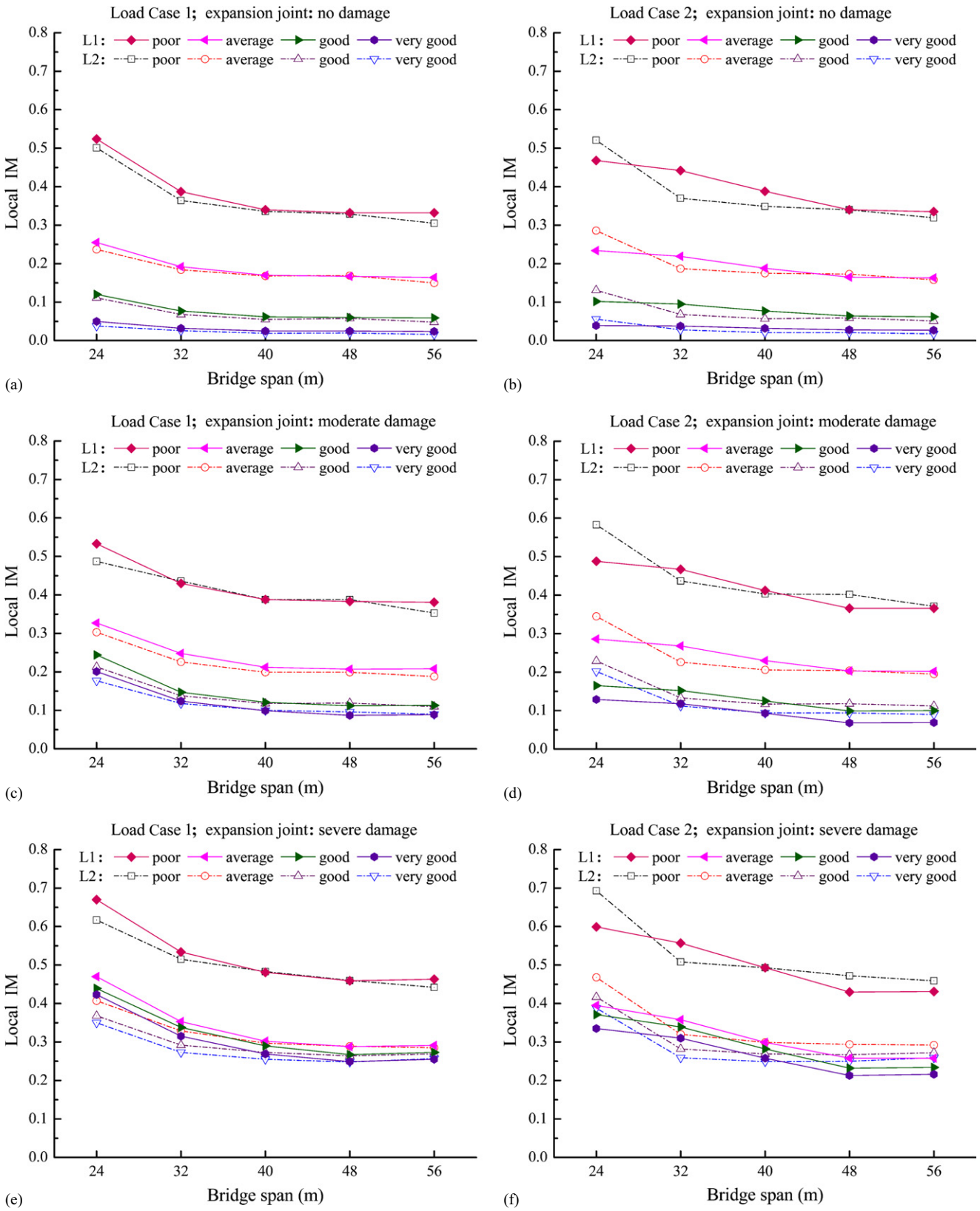

Fig. 8. Local IMs of the deck slab under different road-surface conditions and damage conditions of the expansion joint: (a) Load Case 1, no damage; (b) Load Case 2, no damage; (c) Load Case 1, moderate damage; (d) Load Case 2, moderate damage; (e) Load Case 1, severe damage; (f) Load Case 2, severe damage

From a comparison between the global IMs (Fig. 5) and the local IMs of the deck slab (Fig. 6), it is also found that with no damage in the expansion joint, the local IMs of deck slab are generally smaller than the global IMs, depending on the bridge span length; however, under the severely damaged expansion joint, the local IMs of the deck slab are generally greater than the global IMs. The different trends observed under different damage conditions of the expansion joint occur because the local IMs of deck slab are greatly affected by the damage condition of the expansion joint, which is not the case for the global IMs.

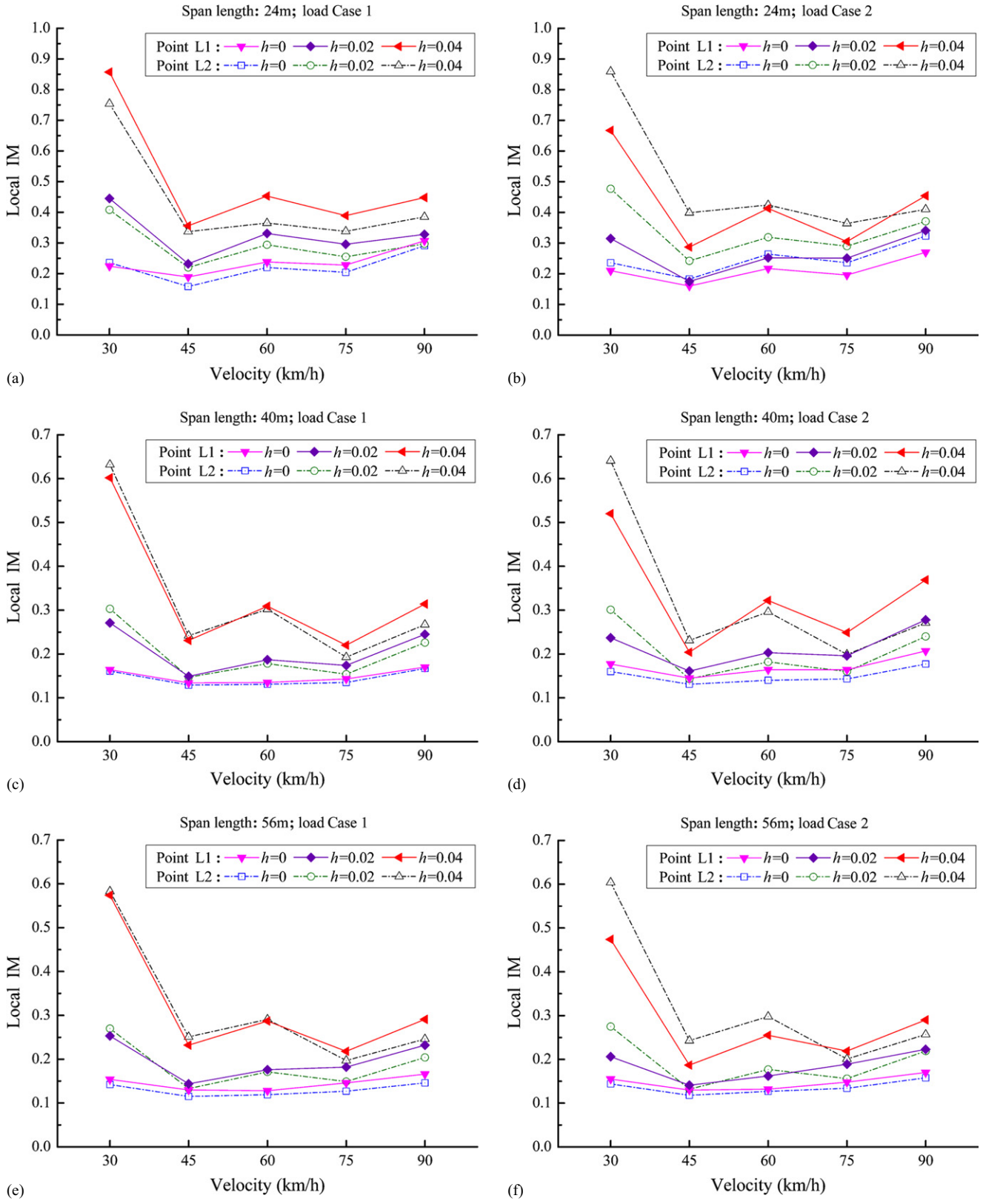

Fig. 9. Local IMs of deck slab versus vehicle speeds: (a) span length = 24 m, Load Case 1; (b) span length = 24 m, Load Case 2; (c) span length = 40 m, Load Case 1; (d) span length = 40 m, Load Case 2; (e) span length = 56 m, Load Case 1; (f) span length = 56 m, Load Case 2

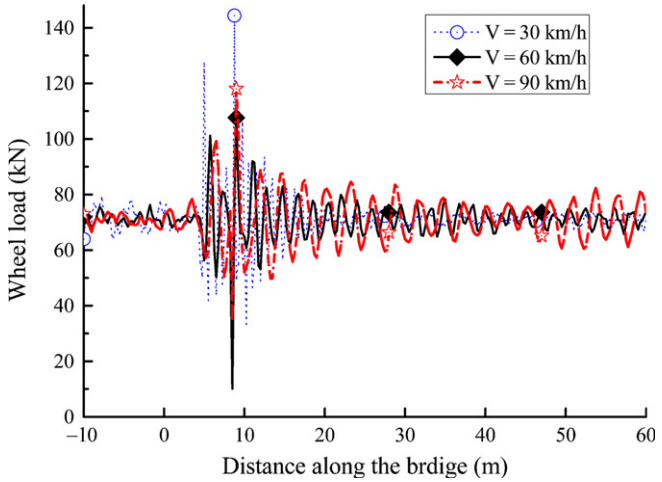

Fig. 10. Wheel-load time history for the rear wheel for different vehicle speeds under a severely damaged expansion joint

Effect of Road-Surface Conditions

The local IMs of deck slab under different road-surface conditions are plotted in Fig. 8 for both load cases and all five bridges. The IM values in Fig. 8 are the averages for the five different vehicle speeds.

From Fig. 8, it can be observed that with no damage in the expansion joint, the local IMs increase notably as the road-surface condition becomes worse. However, as the damage condition of the expansion joint becomes more severe, this increase becomes more difficult to note, especially between the average, good, and very good road-surface conditions. This reveals a fact that the expansion joint itself is an integral part of the road system. Therefore, the deterioration of the expansion joint could significantly affect the dynamic vehicle loading, even if the road-surface condition is very good. In fact, as can also be observed from Figs. 8(e and f), even under very good road-surface condition, the local IMs of the deck slab of the 24-m span bridge can exceed 0.33, the value specified in the AASHTO (2012) LRFD code, under severely damaged expansion joint.

Effect of Vehicle Speed

Many studies have been conducted on the relationship between vehicle speed and IM. The local IMs of the bridge deck are plotted against vehicle speed under different damage conditions of the expansion joint in Fig. 9. Due to the space limitation, only the results of three bridges with span lengths of 24, 40, and 56 m are plotted.

As can be easily seen from Fig. 9, the variation of local IMs with vehicle speed does not follow a certain trend. Similar trends have also been observed in previous studies on the relationship between global IMs and vehicle speed (Deng and Cai 2010b; Green et al. 1995; Broquet et al. 2004). In fact, the effect of vehicle speed on IMs is a very complex issue because it is also affected by many other factors at the same time (Deng et al. 2014). Unfortunately, no consensus has yet been reached on the explanation, despite attempts by many researchers.

In addition, it can be observed from Fig. 9 that under the severely damaged expansion joint, local IMs reach their maxima at a vehicle speed of 30 km/h and these values can far exceed 0.33. To explain this phenomenon, the dynamic wheel load of the rear wheel is plotted in Fig. 10 for three different vehicle speeds under the severely damaged expansion joint. As can be seen from Fig. 10, the largest dynamic wheel load is reached at a vehicle speed of 30 km/h, confirming the results in Fig. 9. This clearly indicates that controlling vehicle speed may not help reduce the dynamic effect of vehicle load on the bridge deck.

Conclusions

In this study, a 3D vehicle–bridge coupled model was developed to study the vehicle impact on the deck slab of concrete box-girder bridges induced by damaged expansion joints. Two concepts were first defined, namely, the local IM of the deck slab, calculated from the deck slab's transverse bending moment, and the global IM, calculated from the deflection and longitudinal bending moment at the bridge midspan. Numerical simulations were carried out and IMs were calculated and compared. The effects of a few important parameters on the local IM of the deck slab were also investigated. The following conclusions can be drawn from this study:

1. The local IMs of the deck slab, for transverse bending moment, increase significantly as the damage condition of the expansion joint becomes more severe. However, the effect of the damage condition of the expansion joint on the global IMs is limited, especially for relatively long bridges.
2. With no damage in the expansion joint, the local IMs of the deck slab are generally smaller than the global IMs, depending on the bridge span length; however, under the severely damaged expansion joint, the local IMs of the deck slab are generally greater than the global IMs.
3. The local IMs of the deck slab due to damaged expansion joints decrease as the bridge-span length increases. In contrast, the global IMs of the bridge do not necessarily follow a certain trend. However, when the bridge's natural frequency was close to the vibration frequencies of the vehicle, resonance may occur and lead to larger global IMs.
4. No specific trend was found on the relationship between the vehicle speed and local IMs due to damaged expansion joints. However, it was found that under a low vehicle speed (i.e., 30 km/h), the local IMs reached their maxima and could be significantly larger than 0.33. This clearly indicates that controlling vehicle speed may not help reduce the dynamic effect of vehicle load on the bridge deck.

The results from this study have clearly indicated the importance of maintaining a good condition of expansion joints to reducing the impact of vehicle loading on the bridge deck. Attention should be paid to the fact that controlling vehicle speed may not be an effective means of reducing the dynamic effect of vehicle load on the bridge deck.

Acknowledgments

The authors gratefully acknowledge the financial support provided by the National Natural Science Foundation of China (Grant Nos. 51208189 and 51478176) and the Excellent Youth Foundation of Hunan Scientific Committee (Grant No. 14JJ1014).

References

AASHTO. (1994). *LRFD bridge design specifications*, Washington, DC.
AASHTO. (2012). *LRFD bridge design specifications*, Washington, DC.
AASHTO-PCI-ASBI (AASHTO-Precast/Prestressed Concrete Institute-American Segmental Bridge Institute). (1997). *Segmental box girder standards*, Washington, DC.
ANSYS 14.5. Computer software, Canonsburg, PA, ANSYS.

Broquet, C., Bailey, S. F., Fafard, M., and Brühwiler, E. (2004). "Dynamic behavior of deck slabs of concrete road bridges." *J. Bridge Eng.*, 10.1061/(ASCE)1084-0702(2004)9:2(137), 137–146.

Brühwiler, E., and Herwig, A. (2008). "Consideration of dynamic traffic action effects on existing bridges at ultimate limit state." *Proc., IABMAS '08: 4th Int. Conf. on Bridge Maintenance, Safety, and Management*, H. M. Koh and D. M. Frangopol, eds., Taylor & Francis, London, 3675–3682.

Deng, L., and Cai, C. S. (2010a). "Development of dynamic impact factor for performance evaluation of existing multi-girder concrete bridges." *Eng. Struct.*, 32(1), 21–31.

Deng, L., and Cai, C. S. (2010b). "Identification of dynamic vehicular axle loads: Theory and simulations." *J. Vib. Control*, 16(14), 2167–2194.

Deng, L., Yu, Y., Zou, Q., and Cai, C. S. (2014). "State-of-the-art review of dynamic impact factors of highway bridges." *J. Bridge Eng.*, 10.1061/(ASCE)BE.1943-5592.0000672, 04014080.

Ding, L., Hao, H., and Zhu, X. (2009). "Evaluation of dynamic vehicle axle loads on bridges with different surface conditions." *J. Sound Vib.*, 323(3), 826–848.

González, A., Cantero, D., and O'Brien, E. J. (2011). "Dynamic increment for shear force due to heavy vehicles crossing a highway bridge." *Comput. Struct.*, 89(23), 2261–2272.

Green, M. F., Cebon, D., and Cole, D. J. (1995). "Effects of vehicle suspension design on dynamics of highway bridges." *J. Struct. Eng.*, 10.1061/(ASCE)0733-9445(1995)121:2(272), 272–282.

Huang, D. (2013). "Impact behavior of concrete bridge deck on girders due to moving vehicles." *Proc., Structures Congress 2013: Bridging Your Passion with Your Profession*, B. J. Leshko and J. McHugh, eds., ASCE, Reston, VA, 689–698.

Hwang, E. S., and Nowak, A. S. (1991). "Simulation of dynamic load for bridges." *J. Struct. Eng.*, 10.1061/(ASCE)0733-9445(1991)117:5(1413), 1413–1434.

ISO. (1995). "Mechanical vibration-Road surface profiles-Reporting of measured data." *ISO 8068: (E)*, Geneva.

Kim, C. W., and Kawatani, M. (2005). "Probabilistic investigation on dynamic response of deck slabs of highway bridges." *Syst. Model. Optim.*, 166(2005), 217–228.

Kim, C. W., Kawatani, M., and Hwang, W. S. (2004). "Reduction of traffic-induced vibration of two-girder steel bridge seated on elastomeric bearings." *Eng. Struct.*, 26(14), 2185–2195.

Kim, C. W., Kawatani, M., and Kwon, Y. R. (2007). "Impact coefficient of reinforced concrete slab on a steel girder bridge." *Eng. Struct.*, 29(4), 576–590.

Lima, J. M., and de Brito, J. (2009). "Inspection survey of 150 expansion joints in road bridges." *Eng. Struct.*, 31(5), 1077–1084.

Schwarz, M., and Laman, J. A. (2001). "Response of prestressed concrete I-girder bridges to live load." *J. Bridge Eng.*, 10.1061/(ASCE)1084-0702(2001)6:1(1), 1–8.

Shi, X., Cai, C. S., and Chen, S. (2008). "Vehicle induced dynamic behavior of short-span slab bridges considering effect of approach slab condition." *J. Bridge Eng.*, 10.1061/(ASCE)1084-0702(2008)13:1(83), 83–92.

Wang, T. L., and Huang, D. (1992). "Cable-stayed bridge vibration due to road surface roughness." *J. Struct. Eng.*, 10.1061/(ASCE)0733-9445(1992)118:5(1354), 1354–1374.

Yin, X. F., Cai, C. S., Fang, Z., and Deng, L. (2010). "Bridge vibration under vehicular loads—Tire patch contact versus point contact." *Int. J. Struct. Stab. Dyn.*, 10(3), 529–554.